

## Neck Muscle Paths and Moment Arms are Significantly Affected by Wrapping Surface Parameters

<sup>a</sup>Bethany L. Suderman, <sup>b</sup>Bala Krishnamoorthy, <sup>a,c,d</sup>Anita N. Vasavada\*

*<sup>a</sup>School of Mechanical and Materials Engineering, Washington State University, Pullman, WA, 99163, U.S.A.; <sup>b</sup>Department of Mathematics, Washington State University, Pullman, WA, 99163, U.S.A.; <sup>c</sup>Gene and Linda Voiland School of Chemical and Bioengineering, Washington State University, Pullman, WA, 99163, U.S.A.; <sup>d</sup>Department of Veterinary and Comparative Anatomy, Pharmacology and Physiology, Washington State University, Pullman, WA, 99163, U.S.A.*

\*Corresponding author. Email: vasavada@wsu.edu

We have studied the effects of wrapping surfaces on muscle paths and moment arms of the semispinalis capitis muscle, one of the major extensors of the neck. Sensitivities to wrapping surface size and the vertebral segment to which it was kinematically linked were evaluated. We found that kinematic linkage, but not radius, had a significant effect on the accuracy of model muscle paths compared to muscle centroid paths from magnetic resonance images (MRI). Both radius and kinematic linkage affected the estimated moment arm significantly. The wrapping surfaces that provided the best match to centroid paths had the most consistent moment arm curves. For some radius and linkage combinations that produced poor matches to the centroid path, a kinematic method (tendon excursion) predicted flexion moment arms in certain postures, whereas geometrically they should be extensions. This occurred because in these cases the muscle length increased as it wrapped around the surface. This study highlights the sensitivity of model moment arms to wrapping surface parameters and the importance of accurately modelling muscle path to obtain better estimates of moment arm.

Keywords: neck muscles, moment arms, wrapping surface, muscle path.

## 1 Introduction

Studies using three-dimensional musculoskeletal models have shown that accurate representation of muscle paths improves model estimates of moment arm, an important determinant of a muscle's mechanical action at a joint. In lower limb (Arnold et al. 2000) and upper limb (Murray et al. 1998, Garner and Pandy 2000) models, muscle paths which curved around geometric objects ("wrapping surfaces" or "obstacle sets") were defined from magnetic resonance imaging (MRI) or cryosection photographs. Compared to straight line paths, model moment arm estimates using these curved paths more closely matched moment arms measured experimentally using the tendon excursion method.

Muscle paths are curved in the human neck as well, but defining the anatomical constraints on muscle paths has been more difficult. Existing neck musculoskeletal models have used via points to wrap neck muscles over bone (Garner and Pandy 2000, Kruidhof and Pandy 2006, Vasavada et al. 1998). This alteration of muscle paths significantly affected model estimates of neck muscle moment arm, force, and moment; and model estimates of neck strength with the altered muscle paths more closely matched experimentally measured neck strength compared to straight path models (Kruidhof and Pandy 2006). However, wrapping muscles over bone does not account for the superficial anatomical constraints provided by soft tissue, and thus other methods are required to model neck muscle paths. A previous study used MRI to define neck muscle centroid paths (the locus of cross-sectional area centroids (Jensen and Davy 1975)) and introduced an objective method for defining and evaluating neck muscle paths using wrapping surfaces in a musculoskeletal model (Vasavada et al. 2008). In that study, modelled muscle paths were validated statically by comparison to centroid paths. However, the analysis of

neck muscle mechanics ultimately depends on the moment arm estimates, which involves modelling neck kinematics. The effect of wrapping surfaces on neck muscle moment arms has not been studied.

Evaluation of model-predicted neck muscle moment arms is difficult because experimentally measured neck muscle moment arms have not been reported. The most common method to determine moment arm is the tendon excursion method; but these experiments are challenging for neck muscles because of the multi-joint kinematics of the spine and muscle attachment sites on multiple vertebrae. However, non-invasive methods have also been used to determine moment arm from images. Geometrically, moment arm of a straight path is defined as the perpendicular distance from the muscle line of action to the instantaneous axis of rotation (IAR) of a joint (An et al. 1984). Moment arm of a curved path has been defined as the shortest distance from the IAR to the centroid path (Wilson et al. 1999). Using this geometric definition, moment arms can be determined from either a series of MRI scans or from the model muscle path geometry, as long as the IAR is also calculated.

In the current study, our goal was to evaluate the effect of wrapping surfaces on model-predicted moment arms of neck muscles. In a multi-joint system, especially when muscles are constrained by superficial soft tissues rather than underlying bones, the choice of wrapping surface parameters are not clear from the anatomy. Because the superficial constraining geometry may change throughout the range of motion, there is not an obvious choice for the size of the wrapping surface. Further, the wrapping surface must be kinematically linked to one rigid body segment (i.e., vertebral body) in the model, and the choice of this linkage affects the position of the wrapping surface in different postures. Therefore, the specific objective of this study was to analyze the sensitivity of neck muscle paths and moment arms to size (radius)

of a cylindrical wrapping surface and the vertebral segment to which it is linked. We evaluated the modelled muscle path by comparison with the centroid path from MRI scans using subject-specific static models in different postures. We assume that accurate representation of muscle paths will lead to improved estimate of moment arm. The effect of wrapping surface size and vertebral linkage was evaluated by estimating model-predicted moment arms using two different methods: (1) a virtual “tendon excursion” method and (2) a geometric method (i.e., shortest distance from the muscle path to the IAR). We hypothesized that both wrapping surface radius and vertebral segment linkage significantly affect neck muscle paths and estimate of moment arm

## **2 Methods**

### **2.1 Muscle paths**

#### **2.1.1 Anatomic paths**

Anatomic muscle paths were obtained from axial MRI scans of a male subject with 55<sup>th</sup> percentile neck circumference (Gordon et al. 1989), as described in a previous study (Vasavada, Lasher, Meyer and Lin 2008). Axial proton density-weighted MR images (TR=2500 ms; TE=18 ms; slice thickness 5.0 mm; gap 1.0 mm) were obtained from the base of the skull to the second thoracic vertebra to identify muscle boundaries. T1-weighted images (TR=400 ms; TE=20 ms; slice thickness 3.0 mm; gap 0.5 mm) were obtained in the sagittal and coronal planes to define vertebral position and orientation. Scans were obtained with the subject in seven different head postures - neutral, 30° flexion, 30° extension, 30° right axial rotation, 20° left lateral bending, 6 cm protraction (anterior translation of the head), and 5 cm retraction (posterior translation of the head). The protocol was approved by the Institutional

Review Board of Washington State University, and the subject provided informed consent.

The anatomic path was approximated by the centroid path (Jensen and Davy 1975) in this study. Neck muscle boundaries were traced on each MRI slice, and the centroid path was defined as a series of straight lines connecting the centroids of cross-sectional areas (CSAs) from consecutive axial slices. A straight muscle path was also modelled between the first and the last centroid points. Results are reported here for the semispinalis capitis muscle (Figure 1), one of the major extensors of the head and neck.

### *2.1.2 Modelled paths and wrapping surface definition*

Subject-specific static models were created using Software for Interactive Musculoskeletal Modeling (SIMM; Musculographics, Santa Rosa, CA). These models reproduced the subject's musculoskeletal geometry in each of the seven head postures from the MRI scans, and were used (1) to define and apply wrapping surfaces and (2) to evaluate the accuracy of the modelled muscle paths compared to the centroid path from MRI (Figure 1). To recreate the subject's posture from the MRI scans, a local coordinate system was defined for each vertebra from midline sagittal MR images. The origin of the local coordinate system was located at the centroid of the four corners of the vertebral body in the sagittal plane. The midpoints of the upper and lower vertebral endplates were identified, and the y-axis was aligned with the two midpoints, positive in the superior (cranial) direction. The x-axis was oriented perpendicular to the y-axis in the sagittal plane and was positive anteriorly; and the z-axis was the cross product of the y-axis and x-axis vectors, positive to the right.

Wrapping surfaces were defined based on the relative positions of the centroid and straight paths in the neutral posture (Figure 1A), such that the straight path was constrained to be closer to the centroid path (Figure 2A). First, the centroid point which was furthest away from the straight path was identified; we assumed that this was the location where the straight path needed greatest adjustment. The x-axis of the cylindrical wrapping surface was defined as the perpendicular direction from the straight path to the furthest point on the centroid path; the y-axis was parallel to the straight path; and the z-axis (long axis of the cylinder) was mutually perpendicular. Although radius was varied in the sensitivity analysis (below), the *target* radius of the cylinder was defined as the distance from the straight path to the furthest centroid point. The centre of the cylinder was placed such that the surface of the cylinder touched the furthest centroid point, i.e., at a distance equal to the cylinder radius from the furthest centroid point to the straight path along the x-axis (Figure 2).

The wrapping surface parameters - cylinder orientation, radius, and centre, were defined separately for the left and right muscles. The values for left and right were averaged to create symmetric wrapping surfaces, which were applied to both the left and right muscles for analysis of the resulting muscle path and moment arm estimates. This step followed from our assumption that the model should be symmetric; averaging the wrapping surface parameters would account for errors due to any asymmetries in the musculoskeletal geometry and possible tracing errors.

### 2.1.3 *Wrapping surface parameter evaluation*

*Radius.* With the cylinder axes described as above, we tested three different values of cylinder radius to evaluate its effect on muscle path and moment arm. The three values for the radius of the cylinder were the target radius ( $r_t$ ),  $0.5*r_t$ , and  $1.5*r_t$  (Figure 2B). A large radius may give a better fit to the centroid path (as measured by

the error metric defined below); this phenomenon is illustrated schematically (in 2 dimensions) in Figure 2B. However, radii that are too large may not provide muscle wrapping in extreme postures, if the endpoint of the muscle is within a wrapping surface. A small radius wrapping surface will not encompass the muscle endpoint in extreme postures, but if it is too small the muscle may not wrap appropriately.

*Kinematic linkage.* We also assessed the effect of linking wrapping surfaces kinematically to different vertebral segments. The vertebral segment chosen for linkage does not change the muscle path in the neutral posture (Figure 3B), but changes how the cylinder rotates in other postures, potentially affecting the muscle path and moment arm over the range of motion (Figures 3A & 3C). The wrapping surface was initially defined in a global coordinate system with the model in the subject's neutral posture. For analysis of other postures, the wrapping surface was defined relative to each of the vertebral local coordinate systems (C1-C7; one at a time) and remained rigidly fixed to that vertebra as the model was placed in other postures.

### 2.1.3 Muscle path evaluation

The quality of the fit between the model wrapped path and MRI centroid path is measured by the *error metric*. The error metric (EM) was previously defined by Vasavada et al. (2008) as the average deviation of the centroid path from the wrapped path, measured at each MRI slice. Although this definition will accurately describe how closely the wrapped path mimics the centroid path overall, it does not discriminate between the cases when the path is within the volume of the muscle or outside it. We assume that physically, the line of action of the muscle should be within the muscle volume (Stokes and Gardner-Morse 1999), so a modelled path that also falls within the muscle volume should be a better representation of the muscle

path. Hence we defined a new error metric that incorporates the muscle boundary along with the original deviation measure.

For the new EM, we determined whether or not the centroid path (point **C** in Figure 4) and the wrapped path (point **W**) are within the cross-sectional area (CSA) for each tracing of the CSA (i.e., at each level) and incorporated a measure of how “well-centred” the point **W** is with respect to the CSA boundary. To this end, we measured the shortest distance from the points, **C** and **W**, to any point on the boundary of the CSA. Let  $d_C$  be the distance of **C** from the CSA boundary and  $d_W$  the corresponding distance for **W** (Figure 4). Assuming **C** (**W**) is inside the CSA, the higher the value of  $d_C$  ( $d_W$ ), the more well-centred **C** (**W**) is. With the original error metric at each level defined as the Euclidean distance  $d$  between **C** and **W**, the new EM is defined for four different cases as follows.

- **Case 1 (Figure 4A).** **C** is **inside** CSA, **W** is **inside** CSA:  $EM = d + (d_C - d_W)$ .  
When both **C** and **W** are inside the cross section, we adjust the error metric value by how much **W** is more well-centred than **C**. EM increases if **W** is closer to the boundary of the CSA than **C** (in this case,  $d_C - d_W$  is positive).
- **Case 2 (Figure 4B).** **C** is **inside** CSA, **W** is **outside** CSA:  $EM = d + d_W$ . In this case, we increase the value of the error metric by the amount that **W** is outside the boundary.
- **Case 3 (Figure 4C).** **C** is **outside** CSA, **W** is **inside** CSA:  $EM = d - d_W$ . It is geometrically possible that a centroid can be outside the CSA. When **C** is outside the CSA boundary (Cases 3 and 4), it is not considered in the calculation of EM as the position of **C** is determined by the shape of the muscle (from MRI data), and not by our method. However, we do adjust the error metric based on the position

of  $\mathbf{W}$  – decrease it when  $\mathbf{W}$  is inside the CSA boundary, and increase it when it is outside (Case 4).

- **Case 4 (Figure 3D).**  $\mathbf{C}$  is **outside** CSA,  $\mathbf{W}$  is **outside** CSA:  $\mathbf{EM} = d + d_{\mathbf{W}}$ .

Notice that for the same  $d$  and  $d_{\mathbf{W}}$  values, the EM in Case 3 will be smaller than that in Case 1 (by  $d_{\mathbf{C}}$ ). This definition captures the fact that the improvement in representation by our method is larger in the former case, where  $\mathbf{C}$  is outside the CSA but our method chooses a  $\mathbf{W}$  that is inside. We observe all four cases in the semispinalis muscle at various postures and slices. We define the overall EM as the average of the EM values over all transverse slices.

Error metric was determined for all combinations of three radii and seven vertebral linkages over all seven postures. For a given combination of radius and linkage, the average error metric over all postures was compared to the error metric provided by the straight path to assess the improvement in muscle path representation. The effect of radius and vertebral linkage on error metric was analyzed using a two-way ANOVA.

## 2.2 *Moment arm*

### 2.2.1 *Generic kinematic model*

Information about intervertebral kinematics between postures, which is necessary for estimating moment arm, was not available from the static MRI scans. Thus, a generic kinematic model of a 50<sup>th</sup> percentile male head and neck musculoskeletal system (Vasavada, Li and Delp 1998) was utilized to evaluate the effect of muscle wrapping on moment arms. The cervical spine has eight intervertebral joints between the skull and T1; at each of these intervertebral joints, the axis of rotation for flexion-extension motions is defined according to radiographic studies (Amevo et al. 1991). The amount of motion occurring at each intervertebral joint was constrained to be a

function of one angle (generalized coordinate) – the angle of the head relative to the trunk.

In the generic model, the straight line path of the semispinalis capitis muscle was defined by its attachments relative to bony landmarks on the skull (midway between the superior and inferior nuchal lines) and vertebra (transverse process of T1). Although the semispinalis capitis has attachments to other vertebrae, its path was simplified for this analysis. Wrapping surfaces defined relative to the vertebral local coordinate system in the subject-specific static model were applied to the kinematic model. The model geometry and posture was slightly different from the subject; therefore, even in the neutral posture there were slight differences in muscle paths depending on the vertebral linkage.

### 2.2.2 *Definitions of moment arm*

In the musculoskeletal modelling software, the moment arm was calculated kinematically using the partial velocity method, equivalent to the change in musculotendon length with respect to head angle:

$$MA = \frac{dl}{d\theta} \quad (1)$$

This kinematic definition of moment arm is the definition used in experimental measurement of moment arm using tendon excursion experiments.

We also calculated the moment arm using a geometric method. The instantaneous axis of rotation (IAR) of the skull with respect to the torso was calculated using the Rouleaux method (Panjabi 1979). The IAR was calculated from 30° flexion to 30° extension at 5° increments. Coordinates of the infraorbital socket and the external occipital protuberance on the skull from the kinematic model in SIMM were recorded at ±2.5° of the desired degree of motion (Figure 5). At each

angle, the extension moment arm was determined as the shortest distance in the sagittal plane from the straight or wrapped path to the IAR (Wilson, Zhu, Duerk, Mansour, Kilgore and Crago 1999).

### 2.2.3 *Moment arm evaluation*

Both kinematic and geometric moment arms were calculated for the straight and wrapped paths. The moment arm was calculated for sagittal plane (flexion-extension) motion, where semispinalis capitis has its largest moment arms (Vasavada, Li and Delp 1998). We evaluated moment arm over a range of 30° flexion to 30° extension because the MRI data covered that range of motion, even though the generic model has a larger range of motion.

As with the evaluation of muscle path, we varied two parameters used in defining the placement and transformation of the cylindrical wrapping surfaces – the radius and vertebral linkage. All possible vertebral linkages (C1 to C7) were examined for each of the three cylinder radii, resulting in 21 moment arm curves. Similar to the error metric analysis, we performed two-way ANOVA tests on kinematic moment arm data to investigate sensitivities to radius and vertebral linkage. For kinematic moment arms, we also reported the standard deviation of moment arm curves for different radii while keeping the vertebral linkage same (7 different standard deviations for each of 3 moment arm curves); and for different vertebral linkages while keeping the radii same (3 different standard deviations for each of 7 moment arm curves). Geometric moment arms are only reported for the target radius with linkages to each vertebra. Therefore, one-way ANOVA tests were performed on geometric moment arm data to investigate sensitivities to vertebral linkage. Paired t-tests were performed to compare kinematic and geometric moment arms at each vertebral linkage (for the target radius only).

### **3 Results**

#### **3.1 Error Metric**

All implementations of wrapping surface radius and vertebral linkage improved the error metric from the straight path (Table 1); the average improvement for all wrapping surface radii, linkages, and postures was 55% (from a straight path error metric of 18.2 mm to an average wrapped path error metric of 8.2 mm). Averaged over all postures, the lowest error metric was 6.6 mm, occurring with the wrapping surface linked to C2 with 50% of the target radius. With this combination (C2 linkage and 50% target radius), the error metric was smallest (4.0 mm) in the neutral posture and largest (12.6 mm) in the lateral bending posture for the contralateral muscle. All five of the lowest error metrics occurred for kinematic linkages to C2 or C3.

For a given wrapping surface radius, the error metric varied significantly depending on the vertebral segment to which the wrapping surface was linked (Figure 6A;  $p = 0$ ). However, for a given vertebral linkage, varying the wrapping surface radius did not significantly affect the error metric (Figure 6B;  $p = 0.75$ ).

While the error metric was affected significantly by the linkage, the variation of error metric with linkage was not uniform over various postures. In fact, the error metric was much larger for linkages to C6 or C7 as compared to other vertebrae for flexion, extension, protraction, and retraction, but varied widely with all linkages for lateral bending and axial rotation (both contralateral and ipsilateral muscles). In order to study the variation with linkage, we calculated the standard deviations for the error metric values for linkages over all radii and to all vertebrae (C1-C7), to C1-C6 (leaving out C7), to C1-C5 plus C7 (leaving out C6), and to C1-C5 (Figure 7). If we discount the large EM values for C6 and C7, we conclude that axial rotation has the

largest variation over all linkages, followed by lateral bending for both contralateral and ipsilateral muscles.

### 3.2 *Moment Arm*

Moment arms calculated using the kinematic method varied significantly with both radius and kinematic linkage (Figure 8;  $p = 0$  for both factors, two-way ANOVA). The moment arm curves vary more with linkages to lower cervical vertebrae, and they also vary more as the radius increases. The geometric moment arm values were calculated for only one radius value, but these moment arms also vary significantly with linkage (Figure 9;  $p = 0$ , one-way ANOVA).

The standard deviation of kinematic moment arm for a given radius over different vertebral linkages increased with increasing radius (Table 2). The standard deviation of moment arm for a given kinematic linkage over different radii was larger as the linked vertebrae were lower in the cervical spine. That is, the upper cervical spine (C1 – C2) had the smallest standard deviation in moment arm for different radii, and the standard deviation increased in the lower cervical spine. Also, standard deviation is larger for the variation of vertebral linkage than for the variation of radius.

For each vertebral linkage, with the radius set to the target radius, kinematic and geometric moment arms were significantly different (paired t-tests,  $p < 0.01$ ). Kinematic moment arms for wrapping surfaces linked to C5, C6 or C7 become negative when the head goes into extension, whereas the geometric moment arms remain positive throughout the range of motion (Figure 9).

The muscle paths resulting in the smallest five error metrics (Figure 10) also resulted in small standard deviation of the moment arm curves (2.128 mm). On the

other hand, muscle paths resulting in the largest **five** error metrics resulted in larger moment arm curve standard deviation (**15.032** mm).

## **4 Discussion**

### **4.1 Muscle paths**

The accuracy of neck muscle paths over a range of postures was not significantly affected by the size of the wrapping surface. We defined the wrapping object such that its surface was at the same location relative to the centroid path in the neutral posture, for any radius. For all wrapping surface radii and linkages, the wrapped muscle paths in the neutral posture were very similar. For different postures, however, each vertebra moved by a different amount. Altering the vertebral segment to which the wrapping surface was linked significantly altered the muscle path over a range of postures.

For the semispinalis capitis muscle, the best muscle paths (lowest error metric) occurred with linkages to upper cervical vertebrae (C2 or C3), whereas the worst paths (largest error metric) occurred with linkages to lower cervical vertebrae (C6 or C7). The motion of the upper cervical vertebrae (in a global coordinate system) are a cumulative sum of the motion of all vertebrae below it. Therefore, wrapping surfaces linked to upper cervical vertebrae moved a greater amount than those linked to lower vertebrae (c.f., Figure 3). For C2 and C3, this appeared to be appropriate to match centroid paths, but wrapping surfaces linked to C1 had higher error metrics. It may be that vertebrae in the mid-region of the neck better represent the overall movement of the neck (i.e., vertebral bodies and soft tissue) that gives shape to the muscle path.

This work shows that, at least for the neck, evaluating multiple postures is important to obtain model muscle paths that accurately represent the musculoskeletal

anatomy. Using data from the neutral posture only, it may not be possible to obtain accurate muscle paths over a range of motion. For example, for this muscle if only the neutral posture was considered, the lowest error metric was the wrapping surface linked to C1 with  $1.5*r_i$ . When averaged over all postures, this combination had an error metric (7.9 mm) which was just below the median of the 21 possible combinations of error metric and radius. In fact, the error metric varied very little in the neutral posture; the standard deviation over all sets of wrapping surface parameters (radius and linkage) was 0.1 mm, making it difficult to choose any set of wrapping surface parameters over the other. However, the standard deviation of error metric over all postures was 3.9 mm, and it is clear that some wrapping surface parameters are superior in non-neutral postures (Figure 3).

As we found in our earlier study (Vasavada, Lasher, Meyer and Lin 2008), modelled muscle paths were least accurate in out-of-sagittal plane postures (i.e, lateral bending and axial rotation). For applications that involve these postures, a different method of selecting wrapping surface parameters may be necessary (for example, a wrapping surface that minimizes the error metric in a particular posture, rather than neutral or minimizing the average error metric over several postures).

In this study, we defined a new error metric to quantify the deviation of the wrapped path from the anatomic path. This new error metric incorporated the distance of the wrapped path from the centroid path, and also to the volumetric boundary of the muscle. For the semispinalis capitis muscle, penalizing the wrapped path for not passing through the CSA at each slice did not ultimately affect the wrapping surface that provided the best fit. However, this could be a significant factor for other neck muscles with more complicated geometry (e.g., the trapezius).

## 4.2 *Moment arm*

Moment arm varied significantly with both linkage and radius, but was more sensitive to linkage. When wrapping surfaces were linked to lower cervical vertebrae, however, there was also more variation in moment arm with respect to radius size. A surprising result of this study was the model prediction of flexion moment arms in extended postures for certain combinations of wrapping surface radius and linkage (Figure 8). These occurred for linkages to lower cervical vertebrae, which did not move as much as upper cervical vertebrae (c.f., Figure 3), so that the muscle lengthened as the head extended, because it wrapped around a larger arc of the surface.

We found differences in the moment arms calculated by a kinematic method (change in muscle-tendon length vs. change in joint angle) compared to those with a geometric method (distance of the muscle path from the joint axis of rotation). For the semispinalis capitis in flexion-extension, we found that geometric estimates of moment arm are positive (i.e., extension moment arms) for all linkage and radius combinations, while kinematic estimates become negative (flexion moment arms) in extended postures for some linkages. We expect the semispinalis capitis acts as an extensor in the cervical spine throughout the range of motion because the IAR is anterior to the muscle path, and the negative moment arm predicted by the kinematic method is physically incorrect for those cases. The wrapping surface parameters which produced negative moment arms are clearly not appropriate parameters, as evidenced by their lack of correspondence to the muscle path (Table 1 and Figure 3). However, these results should serve as a caution; all wrapping surface parameters do not produce appropriate muscle paths, so these paths must be evaluated in multiple postures to select the best wrapping surface. We also found that moment arm

estimates from the tendon excursion and geometric method agree for straight paths and do not agree for curved paths. This may imply that one method or both methods may not be the best choice to determine moment arm for curved paths.

The model-predicted moment arms have not been compared to experimentally measured neck muscle moment arms, because to our knowledge these data are not available in the literature. This study suggests that it is critical to measure neck muscle moment arms by both the tendon excursion (kinematic) method and imaging (geometric) method in cadavers. Tendon excursion experiments are difficult to perform in the neck because of the complex neck muscle anatomy (multiple slips of muscles attaching to different vertebrae) and complex kinematics. Imaging may also be used to measure moment arms *in vivo* in humans, which may provide different results because of muscle tone.

#### **4.3 Relationship between muscle paths and moment arms**

We found that the wrapping surface parameters which produced the best match to muscle centroid path (lowest error metric) resulted in more consistent moment arm curves. According to other studies by Arnold et al. (2000) and Murray et al. (1998), modelling the muscle path accurately should result in the most accurate moment arm estimation. Without experimental measurements of neck muscle moment arms for comparison, we assume that the wrapping surfaces with the best fit to muscle centroid path predicts the most realistic moment arm values.

It is worth noting that radius, which did not significantly alter muscle paths, did significantly affect moment arms. This indicates that even slight differences in modelled muscle path can cause large differences in moment arms. Moreover, even though muscle paths were similar in the neutral posture for different linkages, the moment arms varied greatly.

#### ***4.4 Considerations for selecting wrapping surface parameters***

In this study, we modified our method for selecting wrapping surface parameters that was described in a previous study (Vasavada, Lasher, Meyer and Lin 2008).

Cylindrical wrapping surfaces were previously oriented in the transverse plane when the head and neck were in the neutral posture. Although this method was effective to define muscle paths for most neck muscles, some neck muscles (e.g., trapezius) have more complex paths that would require wrapping surfaces placed in non-transverse planes, or even multiple wrapping surfaces to accurately define the path. Therefore, an alternate method of defining muscle wrapping surfaces was found necessary.

Some of the issues raised in this study may be specific to the type of model we used. For example, the importance of kinematic linkage as a model parameter may be specific to spine models but not important for limb models. Further, we used a subject-specific model to define wrapping surfaces and evaluate muscle paths but a generic model to calculate and evaluate moment arms. Moment arm variation with linkage may have been large because the geometry and kinematics of the generic model were different from the subject-specific models. Even in the neutral posture, muscle paths in the generic model were different with different kinematic linkages, because the vertebrae had different relative positions. We also calculated geometric moment arms from the MRI data in one posture (neutral, using an IAR calculation from the MRI in 30° extension and 30° flexion postures). The moment arm in neutral from the MRI data (subject-specific) was 22 mm, whereas the average geometric moment arm for all kinematic linkages was 34 mm using an IAR calculated at neutral with a 5° range and 31 mm using an IAR calculated with a 60° range (as in the MRI scan). Although lower than the generic model predictions, the subject-specific generic moment arm is in the appropriate range.

## **5 Conclusions**

We found that neck muscle paths and moment arms were significantly affected by the parameters used to define wrapping surfaces. In particular, the vertebral body to which a wrapping surface is linked is a critical parameter in the definition of wrapping surfaces. However, wrapping surface parameters which resulted in a better match to muscle paths also resulted in smaller variations in moment arm curve estimations. We urge caution in selecting the vertebral body to which the wrapping surface is linked and suggest that a range of postures be used to select appropriate wrapping surface parameters.

**Acknowledgements:** We thank Richard Lasher and Travis Meyer. Supported by NSF (CBET #0748303) and the Whitaker Foundation.

## References

- Arnold A, Salinas S, Asakawa D and Delp S. 2000. Accuracy of muscle moment arms estimated from MRI-Based musculoskeletal models of the lower extremity. *Computer Aided Surgery*. 5:108-119.
- Murray WM, Arnold AS, Salinas S, Durbhakula MM, Buchanan TS and Delp SL. 1998. Building Biomechanical models based on medical image data: an assessment of model accuracy. *Lecture Notes in Computer Science*:539-549.
- Garner B and Pandy M. 2000. The obstacle-set method for representing muscle paths in musculoskeletal modeling. *Computer Methods in Biomechanics and Biomedical Engineering*. 3(1):1-30.
- Kruidhof J and Pandy M. 2006. Effect of muscle wrapping on model estimates of neck muscle strength. *Computer Methods in Biomechanics and Biomedical Engineering*. 9(6):343-352.
- Vasavada AN, Li S and Delp SL. 1998. Influence of muscle morphometry and moment arms on the moment-generating capacity of human neck muscles. *SPINE*. 23(4):412-421.
- Jensen R and Davy D. 1975. An investigation of muscle lines of action about the hip: a centroid line approach vs the straight line approach. *Journal of Biomechanics*. 8(2):103-110.
- Vasavada AN, Lasher RA, Meyer TE and Lin DC. 2008. Defining and evaluating wrapping surfaces for MRI-derived spinal muscle paths. *Journal of Biomechanics*. 41(7):1450-1457.
- An KN, Takahashi K, Harrigan TP and Chay EY. 1984. Determination of muscle orientations and moment arms. *Journal of Biomechanical Engineering*. 106:280-282.
- Wilson DL, Zhu Q, Duerk JL, Mansour JM, Kilgore K and Crago PE. 1999. Estimation of tendon moment arms from three-dimensional magnetic resonance images. *Annals of Biomedical Engineering*. 27(2):247-256.
- Gordon CC, Churchill T, Clauser CE, Bradtmiller B, McConville JT and Walker RA. 1989. 1988 anthropometric survey of U.S. army personnel: methods and summary statistics.
- Stokes IAF and Gardner-Morse M. 1999. Quantitative anatomy of the lumbar musculature. *Journal of Biomechanics*. 32(3):311-316.
- Amevo B, Worth D and Bogduk N. 1991. Instantaneous axes of rotation of the typical cervical motion segments: a study in normal volunteers. *Clinical Biomechanics*. 6(2):111-117.
- Panjabi M. 1979. Centers and angles of rotation of body joints: a study of errors and optimization. *Journal of Biomechanics*. 12(12):911-920.

Table 1. Error Metric (mm) averaged over all postures for each combination of radius (rows, given as percentage of target radius) and linkage (columns). The error metric for the straight path averaged over all postures was 18.2 mm.

Linkage	C1	C2	C3	C4	C5	C6	C7
Radius							
50%	8.0	6.6	6.8	7.6	8.1	10.4	12.2
100%	7.9	6.7	6.7	7.1	7.6	9.4	11.4
150%	7.9	6.8	6.7	7.0	7.5	9.2	11.5

Table 2. Standard deviation (S.D.; mm) of moment arm curves, averaged over the range of motion for flexion/extension. Linkage data are the standard deviation over all three radii, and radius data are the standard deviation over all seven linkages.

Linkage	C1	C2	C3	C4	C5	C6	C7
S.D.	0.163	0.791	1.606	3.264	7.864*	8.540*	12.734

Radius	50%	100%	150%
S.D.	16.604	20.266	20.850*

\* Because of the discontinuity in the curves for linkages to C5 and C6 with 150% target radius, the data were only averaged up to the point where the discontinuity occurred (16° for analyses containing C5 and 23° for analyses including C6).

## Figure Captions

Figure 1. Subject-specific model displaying muscle paths in the neutral posture. A. Straight path (yellow) and centroid path (blue), B: Wrapped path (yellow) and centroid path (blue).

Figure 2. Two-dimensional representation of the muscle path and wrapping surface definition. A. Centroid paths (circles), straight path, and wrapping surface with the target radius displaying cylinder axes orientation and the wrapped path. B. Three wrapping surfaces, each with different radii (50%, 100% and 150% of target radius). Wrapped path (not shown for clarity) would be slightly different in each case.

Figure 3. Cross-sectional area (CSA) of the semispinalis capitis on axial slices displaying the different possible locations of the centroid (C) and wrapped (W) path with respect to the CSA. A. Case 1, both the wrapped and centroid path inside the CSA. B. Case 2, centroid path inside the CSA and wrapped path outside the CSA. C. Case 3, Centroid path outside the CSA and wrapped path inside the CSA. D. Case 4, both wrapped path and centroid path outside the CSA.

Figure 4. Instantaneous axis of rotation (IAR) calculation using the Roleaux method for  $-30^\circ$  (flexion) to  $30^\circ$  (extension) at  $5^\circ$  increments. Perpendicular bisectors are shown for  $\pm 2.5^\circ$  about neutral as an example. IARs are shown for all  $5^\circ$  increments between  $30^\circ$  flexion and extension. For reference, the location of the vertebral bodies in the neutral posture are shown.

Figure 5. Subject-specific model with wrapped path (yellow) and centroid path (blue). Top row: with 50% target radius wrapping surface linked to the C2 vertebrae (resulted in smallest error metric). Bottom row: 50% target radius wrapping surface linked to the C7 vertebrae (resulted in largest error metric. A.  $30^\circ$  extension posture. B. Neutral Posture. C.  $30^\circ$  flexion Posture.

Figure 6. Error metric for each posture. A. Error metric for each radius, averaged over all linkages. B. Error metric for each kinematic linkage, averaged over all radii. Error bars reflect the maximum and minimum values observed. The associated standard deviations are plotted separately in Figure 7.

Figure 7. Standard deviations of error metric over linkages (averaged over radii, presented in Figure 6B) for each posture.

Figure 8. Kinematic moment arm estimates throughout  $30^\circ$  flexion to  $30^\circ$  extension for all combinations of linkages and radii solid line = 50%, dash line = 100% and long-dash line = 150% target radius.

Figure 9. Kinematic (dash lines) and geometric (square blocks) moment arm estimates throughout  $30^\circ$  flexion to  $30^\circ$  extension, for all seven kinematic linkages with 100% target radius.

Figure 10. Kinematic (lines) and geometric (square blocks) moment arm estimates for the wrapping surfaces that resulted in the lowest error metrics and the corresponding geometric moment arm estimate.

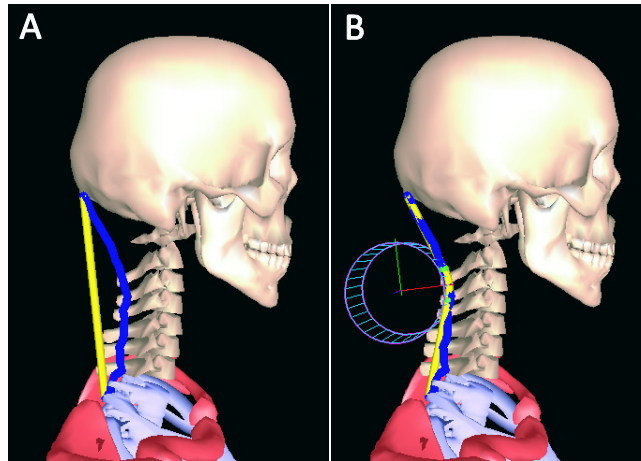


Figure 1. Subject-specific model displaying muscle paths in the neutral posture. A. Straight path (yellow) and centroid path (blue), B: Wrapped path (yellow) and centroid path (blue).

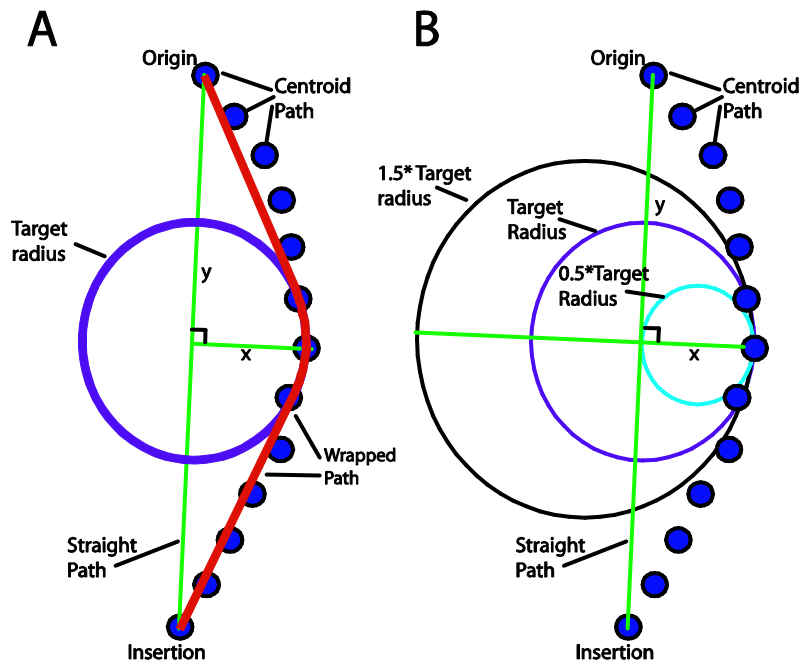


Figure 2. Two-dimensional representation of the muscle path and wrapping surface definition. A. Centroid paths (circles), straight path, and wrapping surface with the target radius displaying cylinder axes orientation and the wrapped path. B. Three wrapping surfaces, each with different radii (50%, 100% and 150% of target radius). Wrapped path (not shown for clarity) would be slightly different in each case.

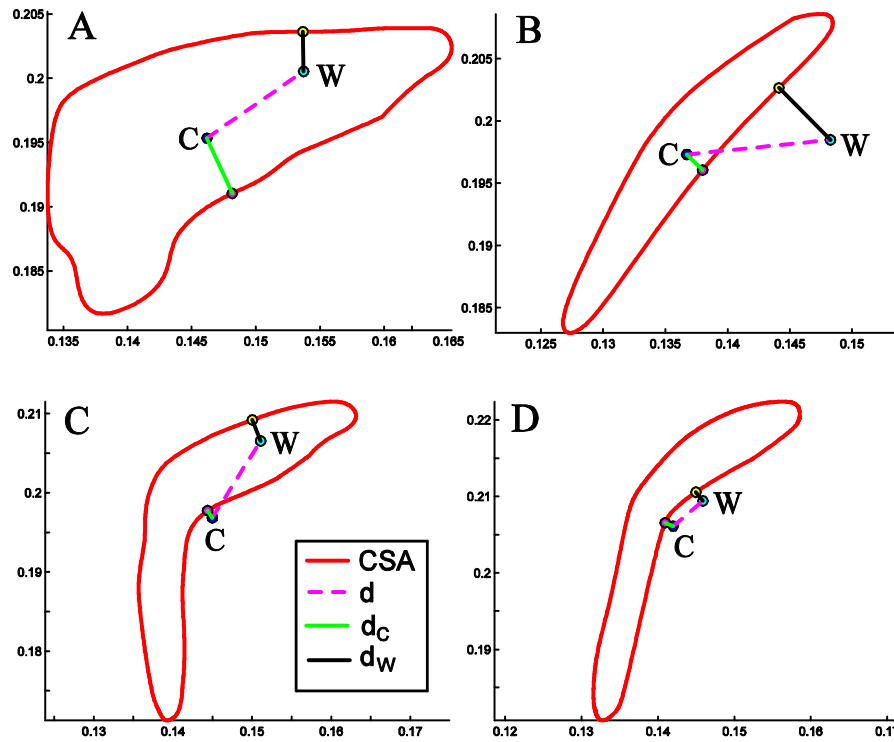


Figure 3. Cross-sectional area (CSA) of the semispinalis capitis on axial slices displaying the different possible locations of the centroid (C) and wrapped (W) path with respect to the CSA. A. Case 1, both the wrapped and centroid path inside the CSA. B. Case 2, centroid path inside the CSA and wrapped path outside the CSA. C. Case 3, Centroid path outside the CSA and wrapped path inside the CSA. D. Case 4, both wrapped path and centroid path outside the CSA.

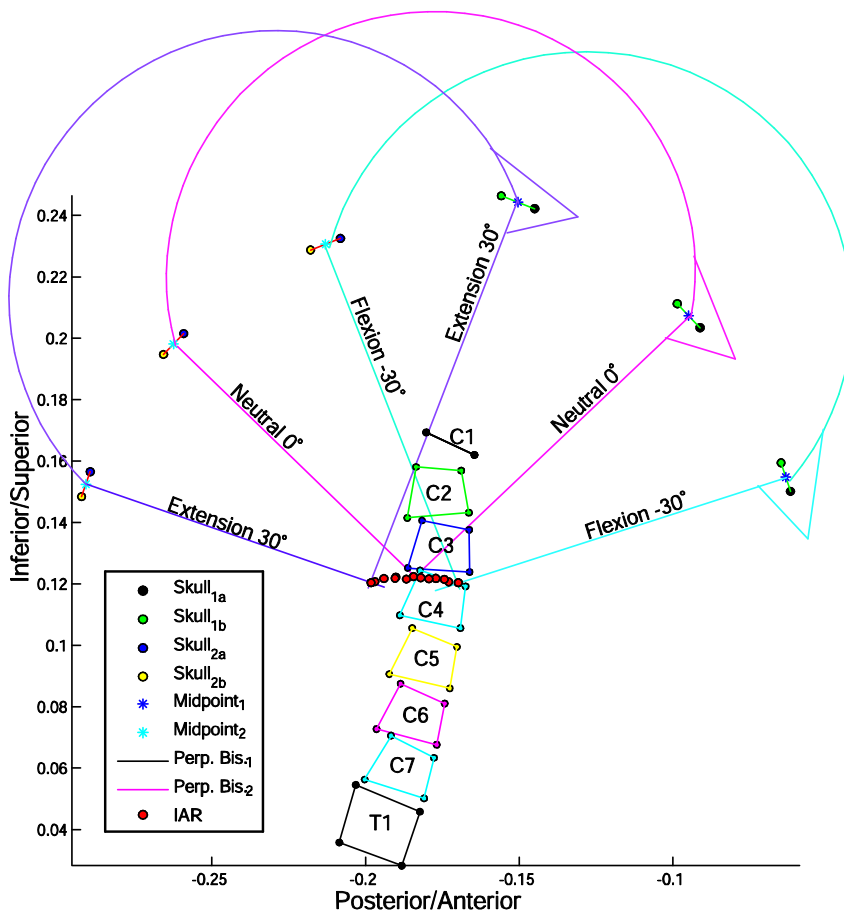


Figure 4. Instantaneous axis of rotation (IAR) calculation using the Roleaux method for  $-30^\circ$  (flexion) to  $30^\circ$  (extension) at  $5^\circ$  increments. Perpendicular bisectors are shown for  $\pm 2.5^\circ$  about neutral as an example. IARs are shown for all  $5^\circ$  increments between  $30^\circ$  flexion and extension. For reference, the location of the vertebral bodies in the neutral posture are shown.

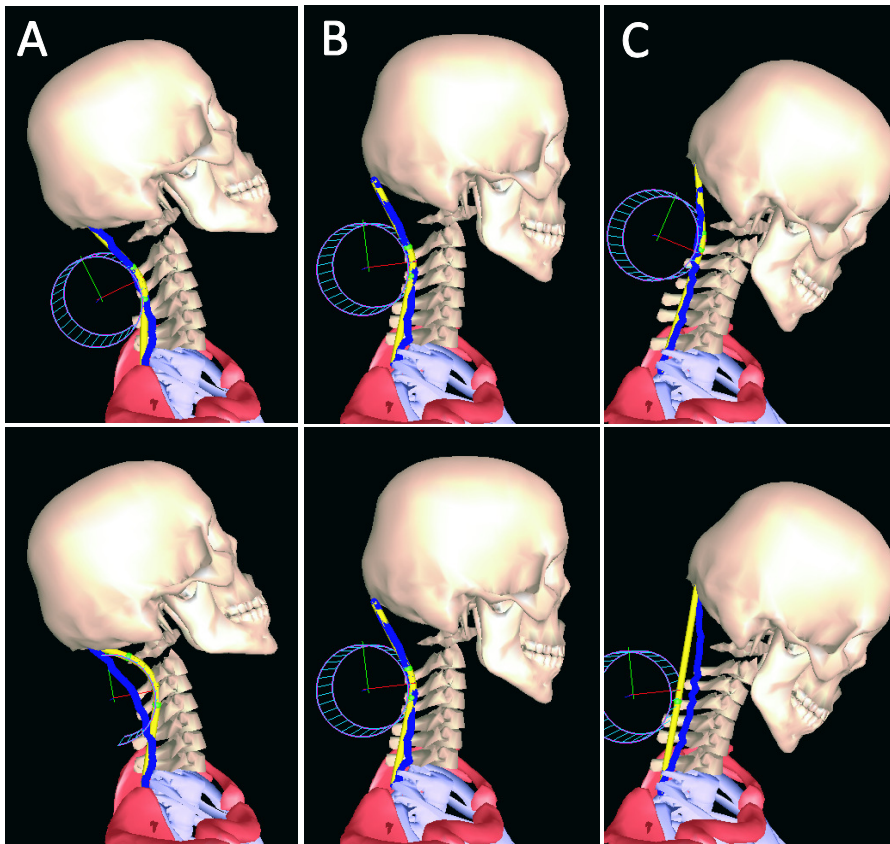


Figure 5. Subject-specific model with wrapped path (yellow) and centroid path (blue). Top row: with 50% target radius wrapping surface linked to the C2 vertebrae (resulted in smallest error metric). Bottom row: 50% target radius wrapping surface linked to the C7 vertebrae (resulted in largest error metric). A. 30° extension posture. B. Neutral Posture. C. 30° flexion Posture.

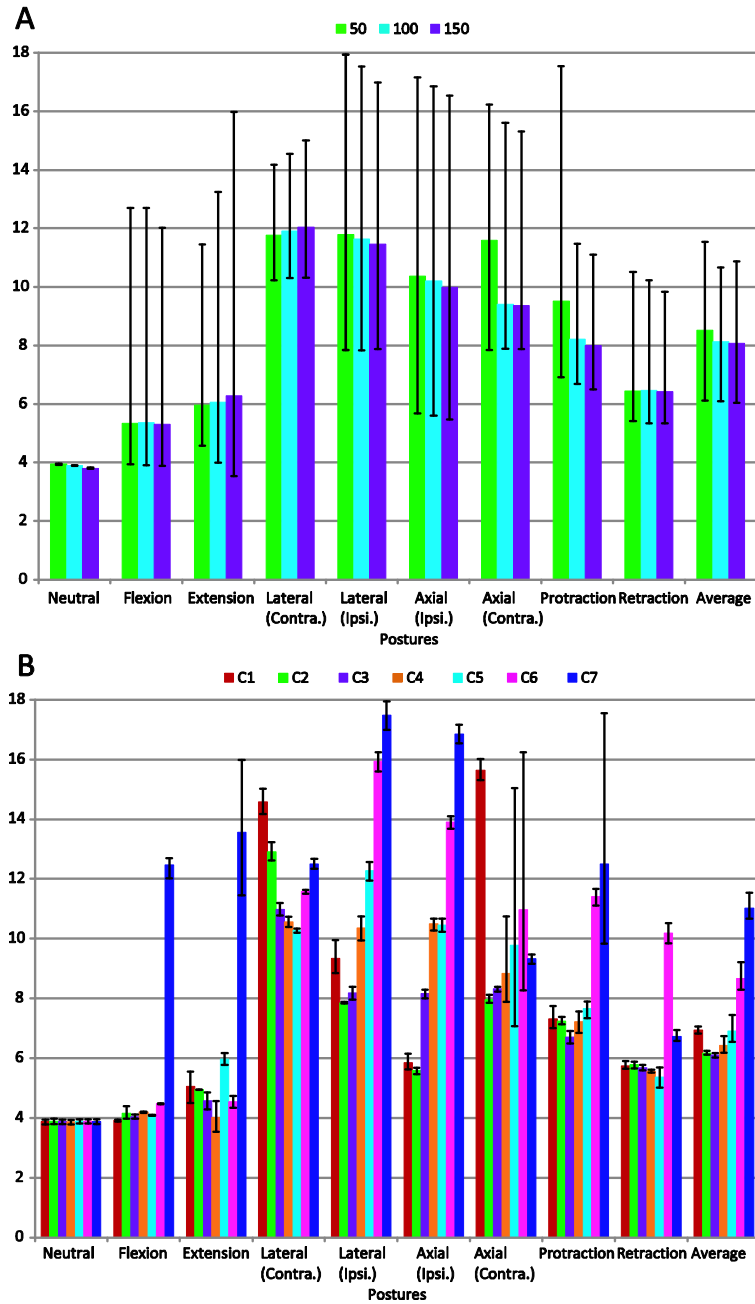


Figure 6. Error metric for each posture. A. Error metric for each radius, averaged over all linkages. B. Error metric for each kinematic linkage, averaged over all radii. Error bars reflect the maximum and minimum values observed. The associated standard deviations are plotted separately in Figure 7.

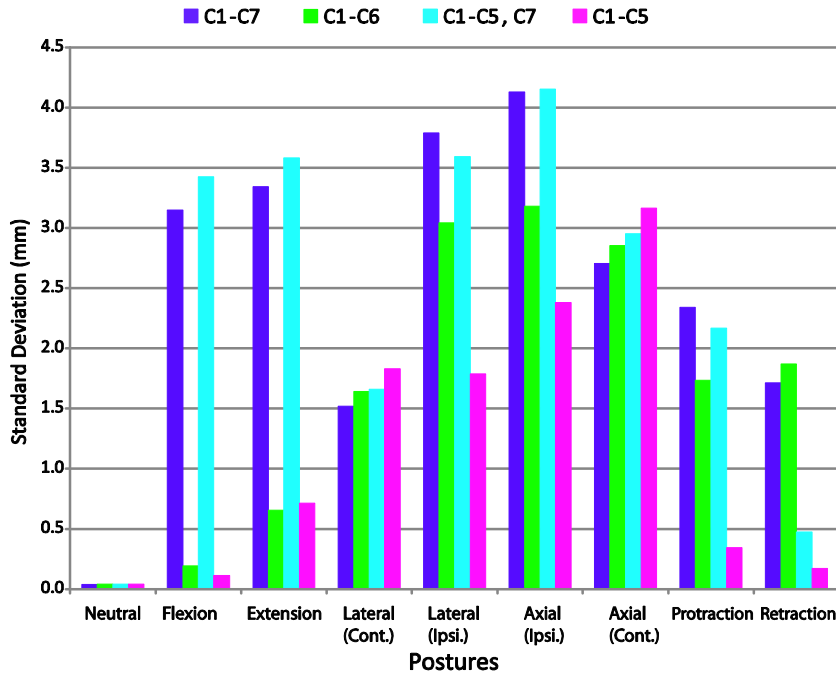


Figure 7. Standard deviations of error metric over linkages (averaged over radii, presented in Figure 6B) for each posture.

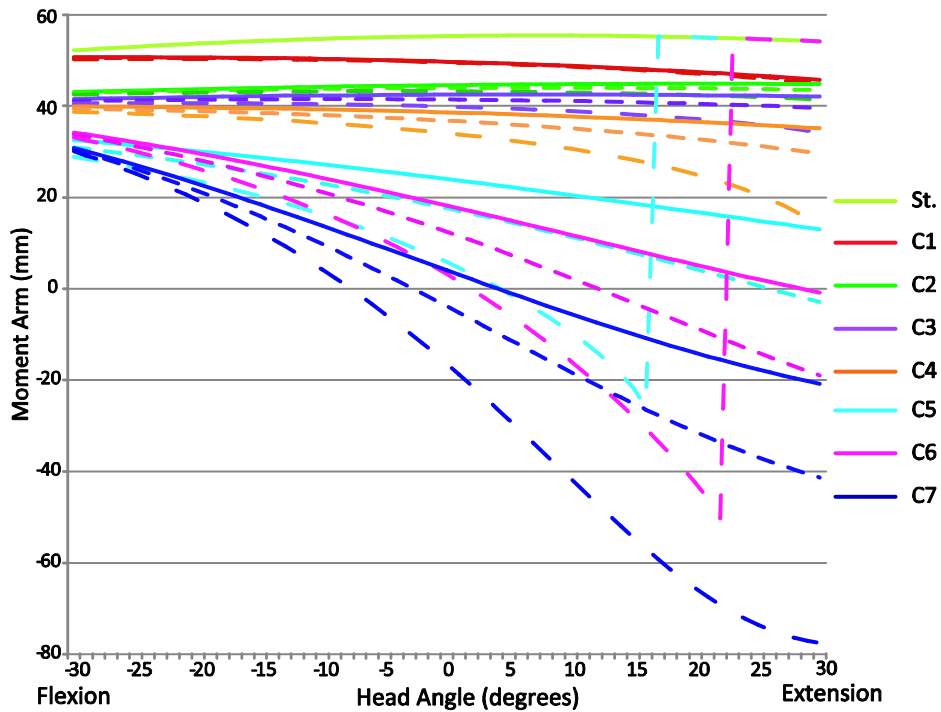


Figure 8. Kinematic moment arm estimates throughout 30° flexion to 30° extension for all combinations of linkages and radii solid line = 50%, dash line = 100% and long-dash line =150% target radius.

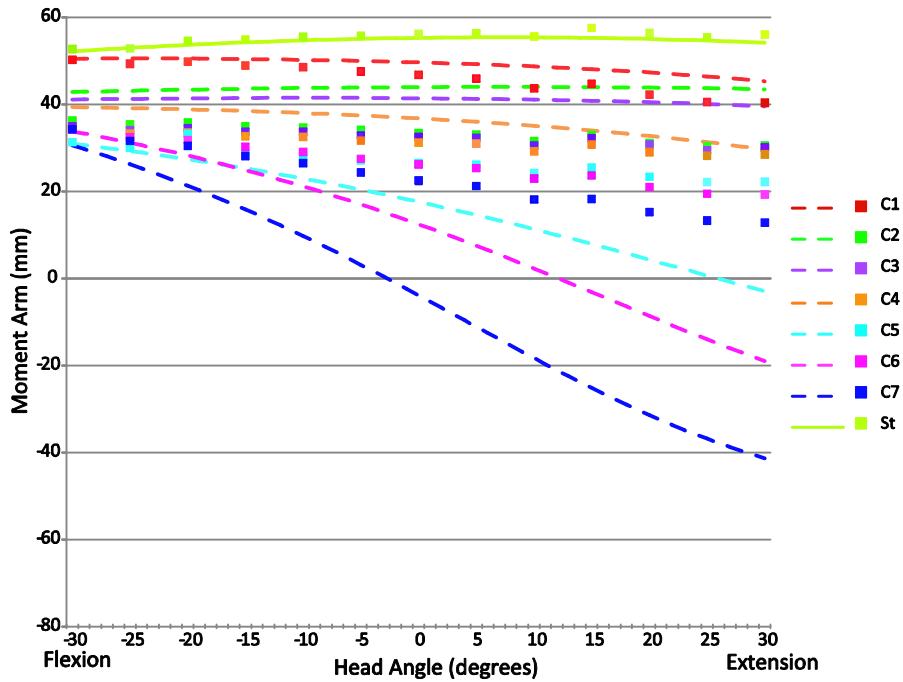


Figure 9. Kinematic (dash lines) and geometric (square blocks) moment arm estimates throughout 30° flexion to 30° extension, for all seven kinematic linkages with 100% target radius.

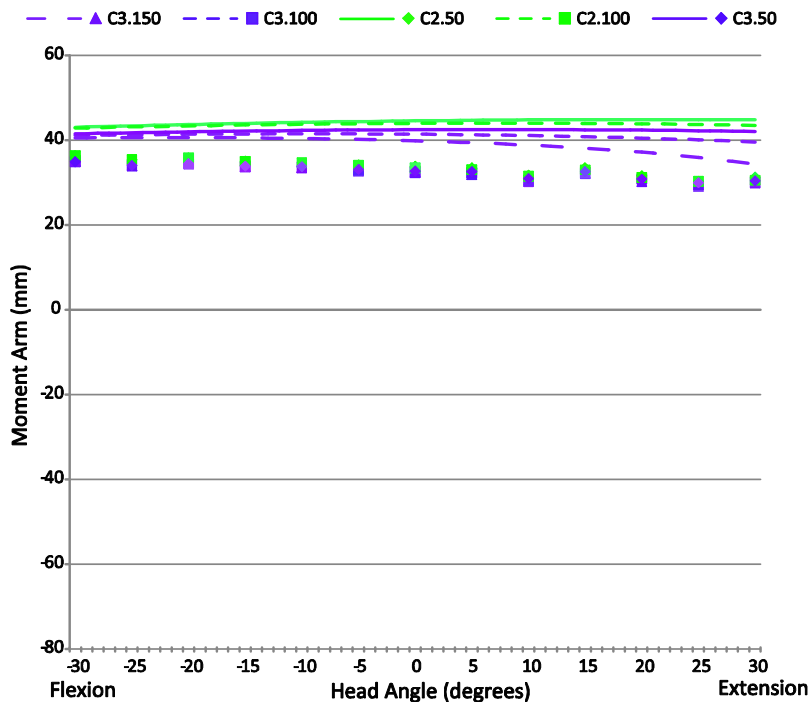


Figure 10. Kinematic (lines) and geometric (square blocks) moment arm estimates for the wrapping surfaces that resulted in the lowest error metrics and the corresponding geometric moment arm estimate.